IEEE Access
Multidisciplinary | Rapid Review | Open Access Journal

Received September 7, 2019, accepted October 22, 2019, date of publication November 4, 2019,
date of current version November 18, 2019.

Digital Object Identifier 10.1109/ACCESS.2019.2951281

A Low-Cost Single-Anchor Solution for Indoor Positioning Using BLE and Inertial Sensor Data

FENG YE, RUIZHI CHEN, GUANGYI GUO, XUESHENG PENG, ZUOYA LIU, AND LIXIONG HUANG

State Key Laboratory of Information Engineering in Surveying, Mapping and Remote Sensing (LIESMARS), Wuhan University, Wuhan 430079, China

Corresponding author: Ruizhi Chen (ruizhi.chen@whu.edu.cn)

This work was supported in part by the National Key Research and Development Program of China under Grant 2016YFB0502200 and Grant 2016YFB0502201, and in part by the NSFC under Grant 91638203.

ABSTRACT Indoor positioning services have become necessary in many situations. Radio frequency (RF) signals are suitable for being used for positioning because of their ubiquity and imperceptibility. This paper utilizes the information from the baseband of a Bluetooth low energy (BLE) transceiver for angle estimation and signal strength for distance estimation. The scheme constitutes a single-anchor based solution to calculate the position of a client. It significantly reduces the cost of installation by avoiding traditional methods like multilateration or triangulation that require three or more anchors, even in a small space. To improve the performance, we design a fusion algorithm based on a Kalman filter to integrate measurements of the anchor station and simplified pedestrian dead reckoning (PDR) results from the client. Experiments show that the proposed solution estimates positions in high precision without initial user location or heading information. The mean error of the implementation is less than 1 m and can be improved to less than 0.5 m with a precise ranging measurement.

INDEX TERMS BLE, data fusion, indoor positioning, Karman filter, pedestrian dead reckoning (PDR), single-anchor.

I. INTRODUCTION

Unlike global navigation satellite systems (GNSS) outdoors [1], indoor positioning technologies cannot be widely applied in practice. There are some basic requirements that indoor positioning systems need to satisfy to make indoor localization becoming a ubiquitous service: accuracy is the most important; convenience refers to the service being easily accessed; inexpensive means the cost must be acceptable for most people.

Different indoor positioning methods are being researched. Some make the most of existing signals indoors, such as GSM [2], [3], geomagnetic fields [4], [5], and Wi-Fi [6]–[8]. The signals also called 'opportunity signals' are not originally for positioning, and can be exploited but cannot work precisely [9]–[11]. Special base stations with the abilities of the Internet of Things (IoT) and positioning are preferred. These devices can be deployed in public buildings without any impacts. Some researchers have focused on improving Wi-Fi devices because of their ubiquitous distribution worldwide. The round trip time (RTT) of 802.11mc has recently attracted focus for its convenient and accurate ranging measurements [12], [13]. At least 3 or 4 stations need to be observed simultaneously at any time. However, too many stations in a building increase cost significantly.

A single-anchor solution that can perform the same work is an alternative. It uses only one base station as the anchor to provide positioning services. For medium-sized spaces, such as exhibition rooms, only one station for positioning is readily accepted because of its convenience of deployment and low cost. Some solutions are dedicated to antenna design, and cannot eliminate signal strength or fingerprinting methods [14], [15]. It increases complexity and cost. Channel state information (CSI) from Wi-Fi devices has the potential for angle of arrival (AoA) estimation [16]. However, the limitations of antenna number and high cost for obtaining measurements make it difficult for practical use. As another signal in 2.4 GHz, BLE is widely used in IoT devices. The low cost and simpler protocol make it suitable to reproduce CSI-based methods [17].

The associate editor coordinating the review of this manuscript and approving it for publication was Liang Hu.

For BLE clients, IMU sensors are often contained, and PDR algorithm can be applied. Fusion algorithms often take advantage of data from the inertial measurement unit (IMU) sensors [18].

This paper proposes a single-anchor solution for indoor positioning, based on the BLE signal and IMU sensors from the client device. The whole solution has the potential to satisfy the requirements of accuracy, convenience, and low cost. Experiments are implemented to evaluate the performance. Tests outdoors show excellent accuracy for angle estimation, and positioning results indoors indicate that the system behaves stably with high accuracy. The main contributions of this paper are as follows:

- We built a low-cost single-anchor system for indoor positioning. The system uses the BLE signal and IMU sensors for position estimation. Additional observations can be easily embedded when needed.
- We implemented a high-resolution angle estimation algorithm with a BLE signal. We analyzed the information from the hardware and constructed the algorithm input.
- We designed a Kalman filter algorithm for data fusion. The algorithm accepts different kinds of observations, including angle and distance estimations. Simplified PDR results from IMU sensors are also integrated.

The paper is organized as follows. Section II reviews some previous work. Section III describes the details of the single station solution. The experiments and analysis of the results are discussed in Section IV. The final Section V presents the conclusion and future work.

II. RELATED WORK

The RF signal is one of the most important sources for indoor positioning [19]. Useful information exposes when the signal transmits from the station antenna to the client antenna, or conversely. They can be translated to position-related measurements. The wide scope from kHz to GHz of a signal contains opportunities for use. Wi-Fi and BLE in the 2.4 GHz band are two of the most closely watched signals because the devices are widely distributed.

For a space with a dense deployment of Wi-Fi or BLE devices, dedicated positioning stations may not be required. Some methods can take full advantage of environmental characteristics. Methods such as fingerprinting [20] are easily implemented because they do not need reconstruction or any modification of the buildings. However, a calibration phase is necessary to construct a database that must be updated periodically. Traditional Wi-Fi fingerprinting based on the received signal strength indicator (RSSI) can achieve an accuracy of 2 to 5 meters, such as RADAR [21] and Horus [22].

Station-based solutions usually modify existing devices, such as Wi-Fi routers, or install new devices, such as BLE beacons. The stations can be used for networking and IoT applications, or only for positioning. The systems are difficult to build but require little maintenance after establishment [23].

Some stations can be used for ranging. RSSI from Wi-Fi or BLE is usually applied. A path loss model is calibrated so that the RSSI readings can be converted to distance related to the station [8], [24]. RTT enhances the ranging capability of Wi-Fi [12], [13]. The 802.11mc protocol defines a mechanism for fine time measurement that can distinguish the short propagation delay of the radio signal and then convert it into distance. UWB is also a time-based technology, which provides precise distance estimations. This kind of measurement is much more stable than the strength-based calculation. With the distance estimations either from RSSI or time-based technologies, a multilateration method is common for position resolving [14]. The accuracy depends on the number of stations. A sub-meter level can be achieved with four or more stations.

For BLE stations, the coverage of the signal is smaller than that of Wi-Fi. The iBeacon defined by Apple based on BLE, can be used for proximity detection, which takes advantage of the short propagation distance [25], [26]. These inexpensive and low energy units can be placed anywhere. Additionally, fingerprinting can be applied. The accuracy of these systems is also related to the device density.

CSI obtained from some Wi-Fi devices is another focus. The information contains the amplitude and phase of the arriving signal. CSI can be used for angle estimation [16], and then a position is calculated by a triangulation method. The same problem is that three or more observations from different anchor stations are required.

Some researchers have attempted to find solutions of single-anchor stations by combining the distance and angle measurements of Wi-Fi. Mariakakis *et al.* [27] uses the time of flight (ToF) observations as a distance basis and improves it with RSSI. PDR is integrated into the system, but AoA estimation is not applied. The mean error is nearly 2 meters. A simulation from Zhi-guo WU *et al.* [28] showed high performance from the fusion of ToF, AoA, and PDR. References [14] and [15] employed a complex antenna design to implement the single-anchor concept based on a 2.4 GHz signal, with an average localization error of 2.32 meters and 1.69 meters, respectively. The methods were not divorced from the signal strength and fingerprinting, and no other sensor data were integrated.

Since the target clients are often smartphones or IoT devices, IMU sensors are common. The PDR algorithm can be applied [18]. As a different type of source, the advantage is that it is a self-contained method and can be isolated from the environment [29]. Using sensors with high performance or mounting them to the foot [30], [31], some improved methods achieve high accuracy with 1% errors of the total distance. Despite the efforts made by researchers, this kind of method requires basic initial conditions. The accumulated error is still an essential problem. Fusion with data from other sensors is a common solution.

BLE and Wi-Fi measurements are frequently used in fusion systems [32]–[38]. Reference [34] obtained estimations from

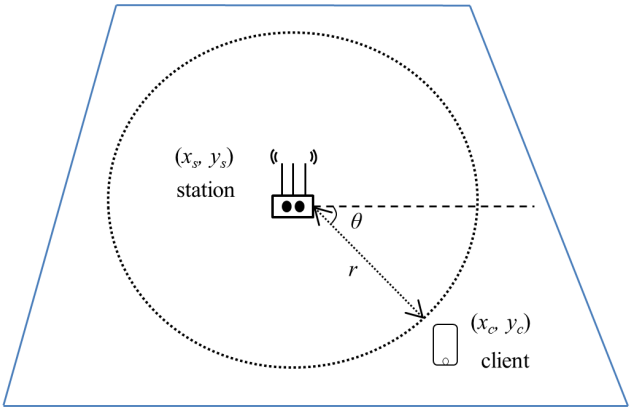

FIGURE 1. Single station based positioning scheme.

a traditional fingerprinting method with a Wi-Fi signal, and a basic and simple weighted average was applied. Reference [35] used an extended Kalman filter to integrate inertial data and position values collected from the nodes of an external fixed infrastructure. The system is implemented on a wearable platform and works well even with absolute position observations at a low rate. The extended Kalman filter was also applied in [36]. Additionally, Bayesian fusion and particle filter are options [37], [38]. Most fusion technology can make the system practical sub-meter accuracy, and increase the robustness of the system.

III. METHODOLOGY

Distance and angle are often concerned within a 2-D indoor positioning system based on a single-anchor station. The anchor is a base station of known position and can be treated as the origin of a polar coordinate system. The distance between the station and the client is as polar radius r, and the polar angle θ represents the angle of the client to station relative to the polar axis. With the position of the station (x_s, y_s), r and θ can uniquely determine the position of the client (x_c, y_c). The relation between them is expressed as

$$\begin{bmatrix} x_c \\ y_c \end{bmatrix} = \begin{bmatrix} x_s \\ y_s \end{bmatrix} + r \begin{bmatrix} \cos\theta \\ \sin\theta \end{bmatrix} \tag{1}$$

Fig. 1 illustrates the positioning scheme. We use the BLE signal to estimate the r and θ. The signal is widely applied in advanced mobile devices, such as smartphones, wearable devices, and many other kinds of IoT devices. Distance and angle measurements can be obtained by analyzing the signal. In detail, distance can be derived via received signal strength (RSS). For angle estimation, a switched antenna array and I/Q samples extracted from the BLE PHY layer are used. These form the basis of the single-anchor solution.

Besides, advanced mobile devices often have considerable computing power and contain a rich set of sensors, such as IMU and magnetometer. The IMU sensors, consisting of a tri-gyroscope and a tri-accelerometer, can be used for estimating attitude and detecting steps of pedestrians. A magnetometer is essential for most devices to find orientation. Additionally, various interfaces such as USB and UART are often provided within these devices. With the interfaces, additional modules can be easily plugged into the devices to extend the sensing ability. All the data from internal sensors or external modules can be processed locally by the powerful CPU of the device.

We demonstrate a single-anchor-based positioning system that takes advantage of a typical mobile device. The performance of the system is tested. In this section, we describe the details of the overall system, as shown in Fig. 2. The system can be divided into an anchor end and a client end.

At the anchor end, the customized base station contains a BLE transceiver equipped with an antenna array. An optional precise ranging master can be added or removed. The antenna array is mainly used for AoA estimation and RSS measurements, and data transmission. The removable ranging module with a capacity of high-precision distance measuring is optional for improving performance. We have currently chosen a pair of inexpensive UWB modules for testing, which can be replaced with any other precise and low-cost ranging units. Therefore, we named it an optional precise ranging (PR) unit of the system. A pair of PR units includes a PR master equipped in the station and a PR client in the mobile device.

For the client end, we utilize a smartphone as the platform of computation and display. It can be replaced with any other advanced mobile devices. A basic PDR algorithm we call simplified PDR is realized based on the indispensable accelerometers and gyroscopes, and the magnetometer is used for initializing heading. An independent BLE transmitter is tied to the smartphone for sending a better and faster signal packet. The built-in BLE antenna of the smartphone is used to receive all BLE-related measurements, including angle α_{AoA} and distance d_{RSSI}. The PR client is plugged into the phone via the USB interface. Distance measurements from the module are transmitted to the host phone in real-time.

With these absolute and relative positioning sources, a fusion algorithm based on a Kalman filter is designed for position estimation. Moreover, the exact heading is estimated for output.

A. AOA ESTIMATION BASED ON BLE

AoA estimation means to determine the impinging direction of a signal arriving at the RF receiver. There are some studies utilizing Wi-Fi CSI for AoA estimation [16], [39]. BLE is also 2.4 GHz signal in the ISM band, which is proven to be an available frequency range for precise measurements [15]. Compared to Wi-Fi, BLE devices are much more inexpensive.

Array signal process technology is used in these systems for finding AoA. For the technology, phases of signals arriving at different antennas are vital measurements. Unlike Wi-Fi's protocol, BLE does not define any quantity related to CSI, from which phase values can be obtained directly. Useful measurements must be extracted from the original I/Q samples, which we can get from the baseband of a low-cost BLE transceiver.

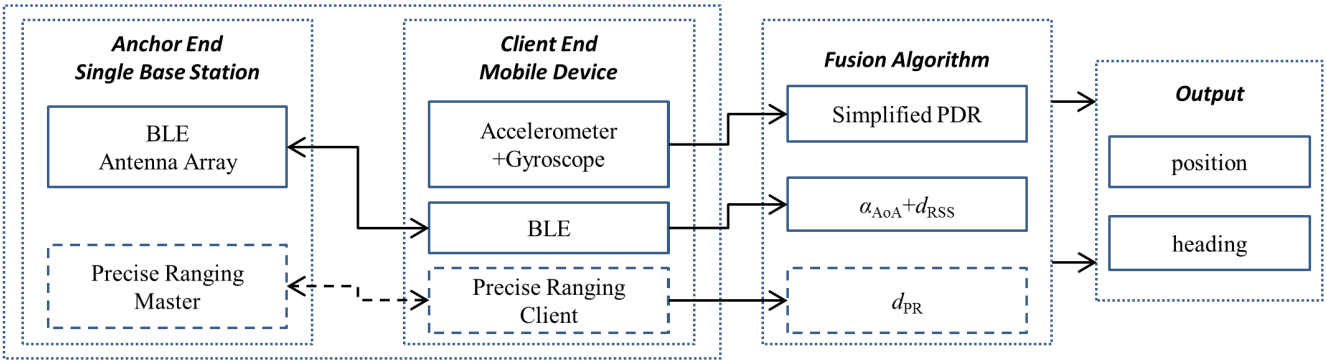

FIGURE 2. Details of the single based positioning solution.

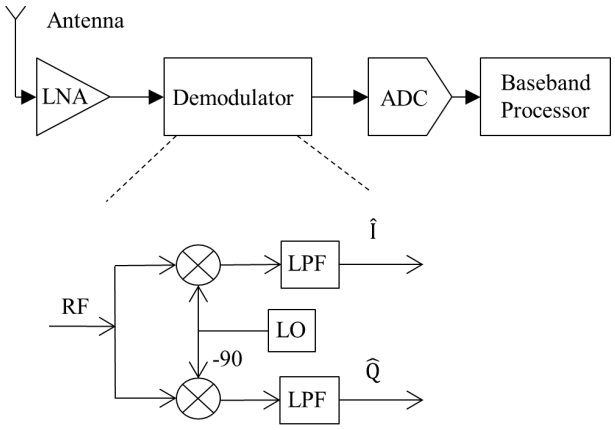

FIGURE 3. A typical signal flowchart of the RF receiver.

1) PHASE MEASUREMENTS FROM THE BLE SIGNAL

For RF systems, radio signals are transmitted or received via an antenna. Modulation and demodulation are necessary before the signals leave or after they arrive at the antenna.

In-phase and quadrature (I/Q) modulation technology is frequently used in these devices. I/Q signals sampled to the baseband can be further processed by a variety of digital methods [40]. Fig. 3 is a typical receiver signal flowchart.

BLE devices share a similar structure. Signals impinging on the antenna are first filtered by a low-noise-amplifier (LNA) and then demodulated into I and Q signals. Actually, a signal with a carrier frequency f_c, phase φ, and amplitude A can be expressed as

$$A\cos(2\pi f_c t+\varphi) = A\cos(2\pi f_c t)\cos(\varphi) - A\sin(2\pi f_c t)\sin(\varphi) \quad (2)$$

Let

$$I = A\cos(\varphi), \quad Q = A\sin(\varphi) \quad (3)$$

Then, the signal can be expressed as

$$A\cos(2\pi f_c t+\varphi) = I\cos(2\pi f_c t) - Q\sin(2\pi f_c t) \quad (4)$$

The expression shows that I/Q can determine the amplitude and phase of the instantaneous state from a signal stream,

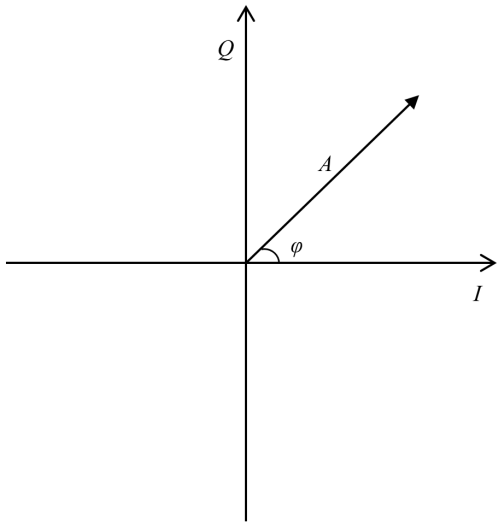

FIGURE 4. Relation between I/Q and signal state.

as shown in Fig. 4. A signal transmitted from an I/Q modulator can be recovered with a demodulator in the receiver. With the I/Q samples from ADC, amplitudes, and phases of arrived signals are estimated in the baseband.

For BLE advertising packets, GFSK modulation is applied, which means that the receiving phase is related to the propagation and modulation frequency of a symbol. Typically, consecutive and stable I/Q samples can be obtained under a fixed environment when transmitting a string of permanent, consistent symbol represented by the frequency Δf_m. The receiving phase φ_r can be expressed as

$$\varphi_r = 2\pi\,\Delta f_m t + \varphi_p = \arctan(Q/I) \quad (5)$$

where φ_p represents the phase shift caused by the propagation, and it is mainly related to the path length and processing delay.

Assuming that consecutive and consistent symbols of an infinite packet are transmitted, switching the currently active antenna while I/Q sampling can obtain measurements with useful characteristics. If the antennas are in the same place, the samples should be the same regardless of which one is selected. When the antennas are placed in order of some

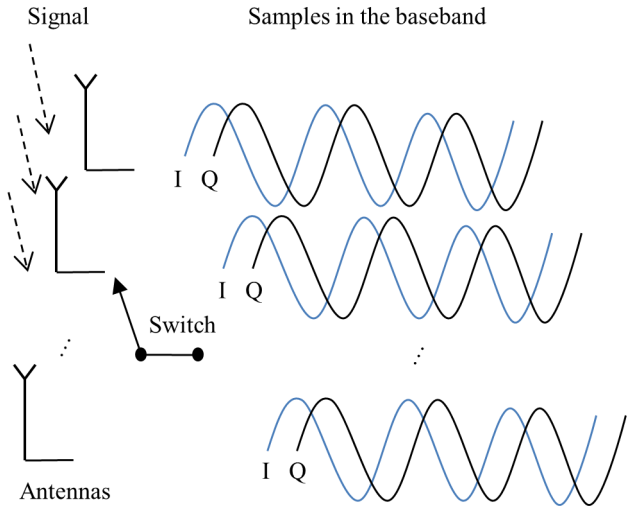

FIGURE 5. Switching antenna for signal receiving.

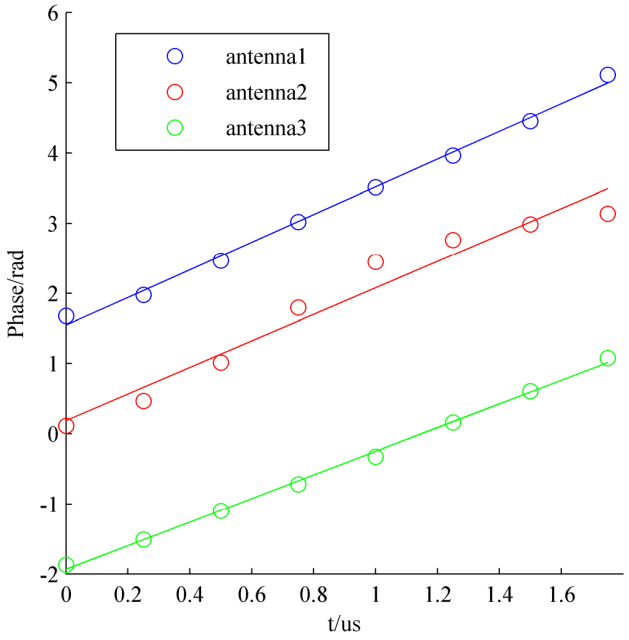

FIGURE 6. Linear fit of received phases.

space, delay appears beginning with the 2nd antenna. The delay is caused by path extension and behaves as the phase shift of the receiving signal. Fig. 5 is intuitive for this mechanism.

For M sequential samples at arbitrary antennas, the m^{th} sample at t$(m-1)$ has a phase of $\varphi_r(m)$. The symbol frequency Δf_m demodulated at different times may be slightly different from the theoretical modulation frequency of 250 KHz for BLE. A linear fit method can be applied to estimate a more precise propagation-related phase φ_{path}. It can be expressed as

$$(\Delta f_m, \varphi_{path}) = \arg\min_{(\rho,\beta)} \sum_{m=1}^{M} (\varphi_r(m) - 2\pi t(m-1)\rho - \beta)^2 \quad (6)$$

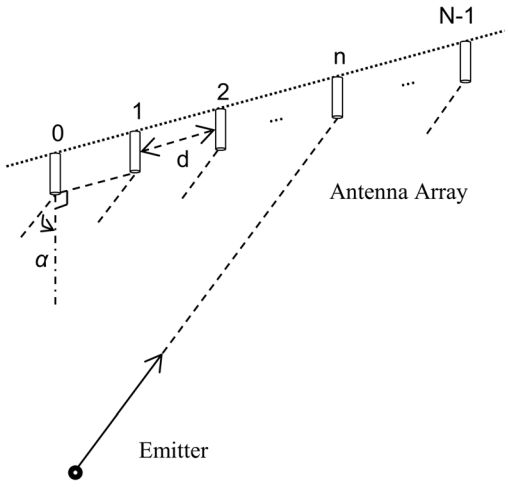

FIGURE 7. Uniform linear array of antennas.

Fig. 6 is an experimental example of phase data from 3 linearly distributed antennas. The transmitter and the receiver are fixed at 5 meters apart.

With the fitting results, a relatively exact estimation of the phase for the real condition can be obtained.

2) AOA ESTIMATION BASED ON A UNIFORM LINEAR ARRAY

With the phase information from a set of antennas, further signal processing can be executed. There have been some efficient methods for AoA estimation with an antenna array system [41]. The antennas are usually arranged into the form of a uniform linear array (ULA) or uniform circular array (UCA).

A ULA is a normal form of antennas placed with a certain space in a line, as shown in Fig. 7. Theoretically, two antennas can accomplish the angle estimation, but three or more are used in practice [42]. UCA is a form of antennas placed in a circle. With this arrangement, the 2-D results of azimuth and elevation can be estimated. However, this kind of form usually requires at least six antennas [43], or more than eight antennas for better performance. A large number of antennas inevitably lead to an increase in the size of the receiver. Also, 2-D computation will require considerable resources.

We use ULA for the low-cost single-anchor system, and exploit the 1-D angle measurement for fusion with ranging and PDR results. Fig. 7 is a ULA with N antennas that are spaced with equal distance d.

For a far-field signal with a wavelength of λ, the arrival angle α is the same for every antenna. The difference in propagation distance between two adjacent elements is $d\cos\alpha$. The spatial distance produces a phase difference of ϕ for the signal propagation, which can be represented as

$$d\cos\alpha = \frac{\lambda\phi}{2\pi} \quad (7)$$

With a pair of phases measured from 2 different antennas m and n, a result can be easily obtained by a simple computation

as

$$\alpha = \arccos(\frac{\varphi_{path/m} - \varphi_{path/n}}{m-n} * \frac{\lambda}{2\pi d}) \tag{8}$$

However, in practice, multipath and noise make the phase measurements too complicated to make the simple relationship effective.

MUSIC is a high-resolution AoA estimation algorithm [44]. With the antenna configuration shown in Fig. 7, the phase shift introduced at n^{th} antenna relative to the 0^{th} is $-2\pi^* n^* \lambda^* d \cos\alpha$. Usually, a complex exponential expression is used for denoting the relationship between the transceiver as

$$\Phi(\alpha) = e^{-j2\pi^* n^* \lambda^* d \cos\alpha} \tag{9}$$

Then, a steering vector can be obtained by

$$\overrightarrow{a}(\alpha) = \begin{bmatrix} 1 & \Phi(\alpha) & \dots & \Phi(\alpha)^{N-1} \end{bmatrix}^T \tag{10}$$

The received measurement matrix $\mathbf{X}$ constructed by sampling results of different antennas can also be represented as

$$\mathbf{X} = \begin{bmatrix} \overrightarrow{x}_0 & \dots & \overrightarrow{x}_{N-1} \end{bmatrix} = \mathbf{AY} \tag{11}$$

where $\overrightarrow{x}_0, \dots, \overrightarrow{x}_{N-1}$ denote the received signal vectors containing phase and amplitude which are all from I/Q values, $\mathbf{A}$ is steering matrix which is comprised of $\overrightarrow{a}(\alpha)$ from multi-sources with different arriving angles of α, and $\mathbf{Y}$ denotes the signal attenuations at each antenna.

With one packet received, several samples from several symbols can be obtained. Since no significant changes occur in the space relationship, we averaged the phases from the symbols in one packet to form a stable and strong measurement. The averaged measurement is treated as one snapshot for the algorithm.

With the MUSIC algorithm, a diagonal covariance matrix $R_{\mathbf{XX}}$ is formed as

$$R_{\mathbf{XX}} = \mathrm{E}(\mathbf{XX}^H) \tag{12}$$

$\mathbf{X}^H$ indicates the conjugate transpose of $\mathbf{X}$. After obtaining the noise subspace E_N by the eigen-decomposition of $R_{\mathbf{XX}}$, construct the spatial spectrum

$$P(\theta) = 1 \Big/ (a^H(\theta) E_N E_N^H a(\theta)) \tag{13}$$

A spectrum peak represents an AoA estimation. With a multipath effect, several top peaks are observed. The independent peaks are separated, and only one peak represents the real angle of the direct path. Considering that the observation of the actual angle should be consecutive for a dynamic test, we discard angles with significant differences with the estimated system states.

Physically, the number of antennas must be larger than the number of propagation paths [16]. For a typical office scenario, ULA with no more than six antennas is acceptable because typically, we can observe five significant paths at most [45].

The number of snapshots is also an important parameter for the final result. It is a balance of accuracy and real-time performance.

B. RANGING BASED ON RSS

RSS is a general reference to the signal propagation distance. Typically, the transmitter is distant when the signal is weak. Many studies focus on the path loss model based on RSSI, which is reported directly in most RF systems [8], [24]. The model describes the relationship between the distance and RSSI value as

$$\hat{d} = 10^{(R^0 - \mathrm{RSSI})/10\gamma} \tag{14}$$

where R^0 is the RSSI at a 1-meter distance, an γ is a factor related to the environment and antenna gain. With the model, calibration also needs to be implemented in advance.

For a practical application, some measurements lead to overwhelmingly large results with the exponential model. The results are not applicable and should be discarded. Otherwise, the filter system might break down. According to the experimental environment, we set 15 meters as the maximum estimation in our implementation.

C. SIMPLIFIED PEDESTRIAN DEAD RECKONING

Mobile devices contain micro-electro-mechanical systems (MEMS) IMUs, which are often small-size and low-cost. Many researchers are working on advanced PDR algorithms with IMU [29]–[31], which improve accuracy by applying complex methods to noisy data from the sensors. However, the system based on IMUs will not return when the trajectory deviates, and prior information is often necessary for initialization.

Since PDR is rarely used individually for absolute positioning, simplifying the algorithm to save energy should be considered for real-time applications. Thus, reconsidering PDR is the direction of our solution. We leverage the low-cost IMU of mobile devices to implement a simplified PDR that can be used for fusion.

There are some key stages in the PDR algorithm, including step detection, step length estimation, and heading estimation. With the step length l_S and heading θ_{hd}, the current position (x_k, y_k) can be updated from the last position (x_{k-1}, y_{k-1}) when a step is detected,

$$\begin{bmatrix} x_k \\ y_k \end{bmatrix} = \begin{bmatrix} x_{k-1} \\ y_{k-1} \end{bmatrix} + l_S \begin{bmatrix} \cos(\theta_{hd}) \\ \sin(\theta_{hd}) \end{bmatrix} \tag{15}$$

Various algorithms can be used to improve the relative accuracy of the position. They focus on estimating the adaptive step length with a refined model [46] or limiting the accumulated error of heading [31].

Different from these PDRs, we consider heading variation and step velocity for fusion. The position relationship can be expressed in the time domain as

$$\begin{bmatrix} x_t \\ y_t \end{bmatrix} = \begin{bmatrix} x_{t-1} \\ y_{t-1} \end{bmatrix} + v_S{}^* \Delta t \begin{bmatrix} \cos(\theta_{hdt-1} + \Delta\theta_{hd}/2) \\ \sin(\theta_{hdt-1} + \Delta\theta_{hd}/2) \end{bmatrix} \tag{16}$$

v_S denotes the scalar velocity of the pedestrian, we use a step length of fixed 0.7 meters so that the velocity is related to the step interval. We simply assume that the velocity remains constant during the gap of two steps. θ_{hdt-1} is the heading at

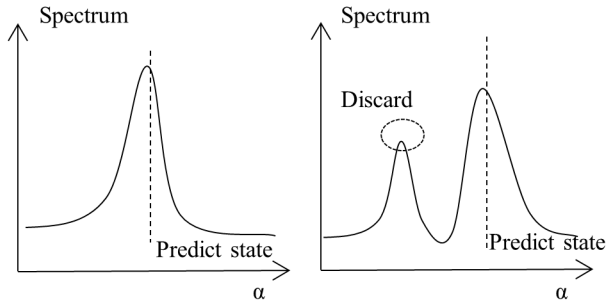

FIGURE 8. Gross error discarding.

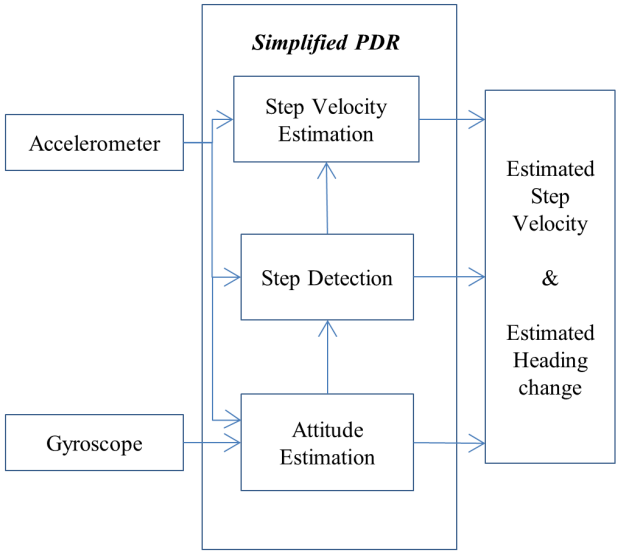

FIGURE 9. Structure of the simplified PDR.

$t-1$, and it is estimated by the filter but not directly obtained from the IMU subsystem. We use the heading variation $\Delta\theta_{hd}$ as an observation for updating the heading. We consider the variation dependable for a short time.

The position output from PDR is ignored since the target position is set as a system state which means that we use only the algorithm to obtain some observations for fusion. They are heading variations and step velocities. The input and output can be described, as shown in Fig. 9.

To obtain these quantities simply, we accept a rough accuracy since errors from observations are common. The method of step detection is to use the total magnitude of the tri-accelerometer. In detail, select the peak of the magnitude preprocessed with a low pass filter and compare the peak with a threshold.

For the heading change, we use a quaternion update method with tri-gyro measurements (ω_x, ω_y, ω_z)

$$\dot{\mathbf{q}} = \frac{1}{2}\begin{bmatrix} 0 & -\omega_x & -\omega_y & -\omega_z \\ \omega_x & 0 & \omega_z & -\omega_y \\ \omega_y & -\omega_z & 0 & \omega_x \\ \omega_z & \omega_y & -\omega_x & 0 \end{bmatrix}\begin{bmatrix} q_0 \\ q_1 \\ q_2 \\ q_3 \end{bmatrix} \tag{17}$$

The relation between the heading angle θ and quaternion $\mathbf{q}$ is given by

$$\theta = \arctan\left[\frac{2\left(q_0q_3 + q_1q_2\right)}{1 - 2\left(q_2^2 + q_3^2\right)}\right] \tag{18}$$

With the change time, which is equal to the fusion update period Δt, the heading change observation from PDR is obtained by

$$\Delta\theta_{hd} = \theta_t - \theta_{t-\Delta t} \tag{19}$$

The key in our application is that the simplified PDR performs a simple algorithm and outputs variation values. The values do not accumulate error or require high-performance sensors that are only equipped in advanced and expensive devices.

For comparison, we also utilized these intermediate quantities to derive a completed PDR result.

D. INTEGRATION OF IMU SENSORS AND BLE SIGNALS

The distance and angle measurements from BLE can determine an absolute position but with significant error, especially the observation from RSSI, which is typically poor. PDR provides fine relative observations for a short time. A fusion scheme based on a Kalman filter is designed to integrate all of these useful measurements. In addition, ranging measurements from the optional PR module can be applied when necessary.

We choose position (x, y), walking speed v, heading θ_{hd}, and heading change rate ω_{hd} as the system states. Then, the system state vector $\mathbf{S}_t$ is expressed as

$$\mathbf{S}_t = \begin{bmatrix} x & y & v & \theta_{hd} & \omega_{hd} \end{bmatrix}^T \tag{20}$$

Since the state transition during the period Δt is not linear as

$$\mathbf{S}_t = \mathbf{S}_{t-1} + \begin{bmatrix} v\cos\theta_{hd} \\ v\sin\theta_{hd} \\ 0 \\ \omega_{hd} \\ 0 \end{bmatrix}\Delta t \tag{21}$$

The linear state transition matrix $\mathbf{A}_j$ is derived as

$$\mathbf{A}_j = \begin{bmatrix} 1 & 0 & \Delta t\cos\theta_{hd} & -v\Delta t\sin\theta_{hd} & 0 \\ 0 & 1 & \Delta t\sin\theta_{hd} & v\Delta t\cos\theta_{hd} & 0 \\ 0 & 0 & 1 & 0 & 0 \\ 0 & 0 & 0 & 1 & \Delta t \\ 0 & 0 & 0 & 0 & 1 \end{bmatrix} \tag{22}$$

AoA, ranging measurements, and PDR results construct observation vector with

$$\mathbf{Z} = \begin{bmatrix} \alpha_{AoA} \\ d \\ v \\ \omega_{hd} \end{bmatrix} = h(x) = \begin{bmatrix} \arctan(\frac{y-y_s}{x-x_s}) \\ \sqrt{(x-x_s)^2 + (y-y_s)^2} \\ v \\ \omega_{hd} \end{bmatrix} \tag{23}$$

where d can be from RSSI as d_{RSSI} or PR as d_{PR}, or both. Moreover, d and α_{AoA} can be from one or more anchor

stations if they exist. That means the length of the observation vector is variable, which depends on the number of observations. Also, the relationships are the same as described in (23), respectively.

The noises of measurements are assumed as Gaussian models. The measurement noise covariance matrix is set based on statistics magnitude extracted from samples with some simple experiments and is adjusted according to the actual results.

Step velocity is derived from the step length l_S and step interval Δt_{step} with

$$v = l_S / \Delta t_{step} \tag{24}$$

The heading change rate is the average heading change in the last period

$$\omega_{hd} = \Delta\theta_{hd} / \Delta t \tag{25}$$

The state is initialized with measurements. In detail, an accelerometer is used to find the pitch and roll angle under static conditions, and a magnetometer indicates the orientation of the phone as the initial heading θ_{hd_0}. AoA and ranging construct the initial position (x_0, y_0). Then, the initial state can be expressed as

$$S_0 = \begin{bmatrix} x_0 & y_0 & 0 & \theta_{hd_0} & 0 \end{bmatrix}^T \tag{26}$$

The error covariance matrix is initialized by the identity matrix as

$$P_0 = \begin{bmatrix} 1 & 0 & 0 & 0 & 0 \\ 0 & 1 & 0 & 0 & 0 \\ 0 & 0 & 1 & 0 & 0 \\ 0 & 0 & 0 & 1 & 0 \\ 0 & 0 & 0 & 0 & 1 \end{bmatrix} \tag{27}$$

IV. EVALUATION AND ANALYSIS

Some experiments were implemented with customized hardware to evaluate the performance of the proposed solution.

The station consisted of a low-cost commercial BLE transceiver and a switched array of six rod antennas that could also be replaced with inexpensive and small-size antennas. Although six antennas were equipped, different configurations with as few as three were tested. The antennas were spaced at 6.2 cm, which was nearly half-wavelength, as shown in Fig. 10. The AoA algorithm was processed in a laptop which served as a server.

The BLE transmitter was a customized beacon equipped with a rod antenna and was treated independently as a signal source. It was tied to a Huawei Mate 20 smartphone. The phone had an Android 9.0 platform with a Kirin 980 processor. An optional UWB module was plugged into the USB port. All measurements were converted with a regular timeline. The built-in BLE module of the phone was used for data exchange.

Experiments were implemented in different environments. An outdoor implementation was for verifying the validity of the BLE AoA algorithm and indoor for evaluation of positioning performance.

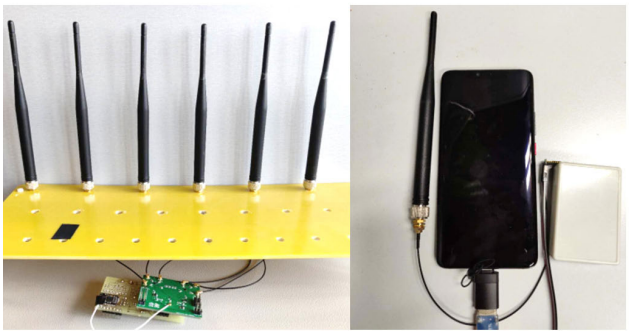

FIGURE 10. Antenna array and test client.

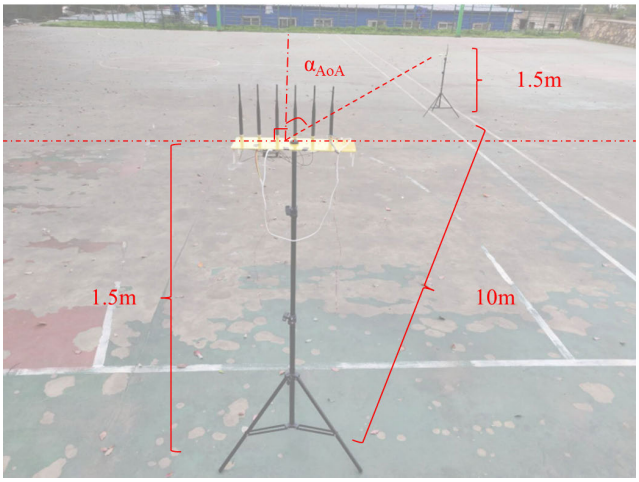

FIGURE 11. Outdoor test.

A. ANGLE ESTIMATION EVALUATION

For an outdoor scene, the multipath effect was not obvious in the open spaces. It is suitable for evaluating the angle estimation method.

The transmitter and the station were placed apart from 10 m for the test, and they were at the same height of 1.5 m from the ground, as shown in Fig. 11.

We collected data at 19 different locations which were spaced 10°. It required over 30 seconds, and more than 300 packets were received at each location. Phases from 6 antennas were recorded, so different configurations of numbers of antennas could be evaluated with the MUSIC algorithm.

For the individual angle measurement, no multipath mitigation efforts were made. The most obvious peak was treated as the only estimation of AoA. Three packets as snaps were fed into the algorithm. Then, 100 estimations were obtained at each location. The process was applied with six antennas and three antennas. All the results are shown in Fig. 12.

Fig. 13 shows the cumulative distribution function (CDF) for the absolute error of the results.

It can be seen that the high-resolution AoA algorithm is efficient over the range of -80° to 80° with six antennas. Most of the results were close to the ground truth, so a simple average method could be applied to obtain more precise estimations for static measurements. Within the range of -

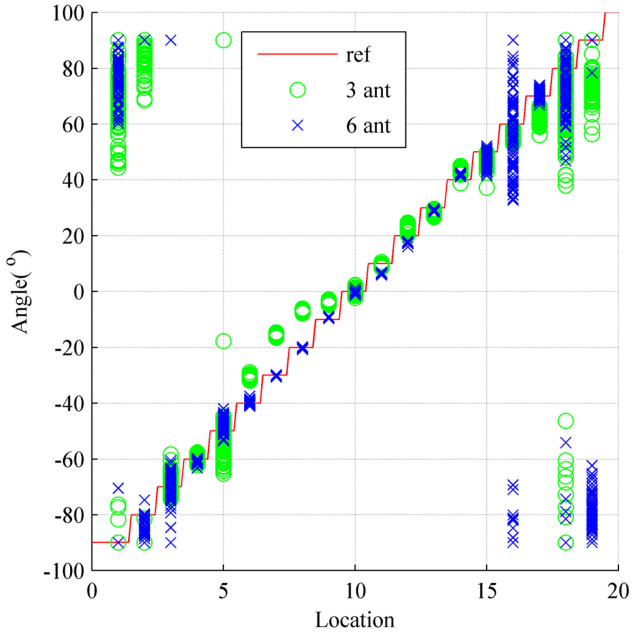

FIGURE 12. AoA estimations from outdoor test.

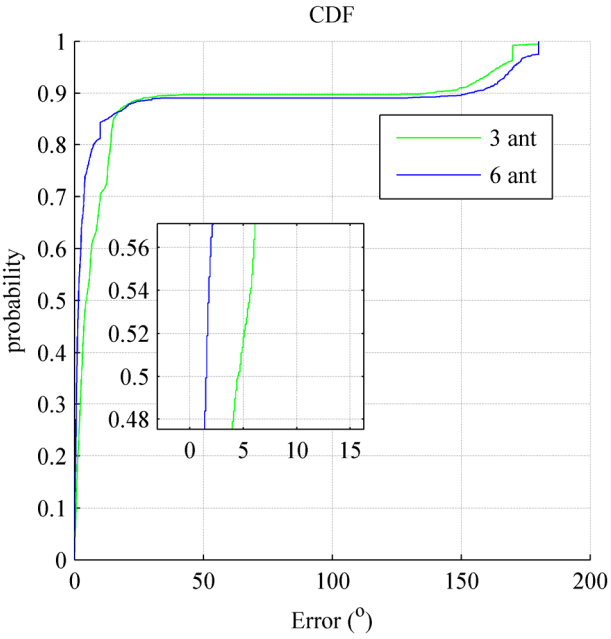

FIGURE 13. CDF of estimations outdoors.

40° to 40°, the variation in estimation error was less than 5°. Therefore, we can conclude that the estimation results with six antennas are precise and stable in a relatively ideal environment.

Fewer than four antennas still worked outdoors, but the performance significantly decreased. For large angles, the results decreased more quickly than with 6 antennas. The results for small absolute angles that were less than 50° were stable but had large bias errors. We think the reason lies in the multipath and some system errors. A configuration of fewer antennas has lower tolerances for the calibration error.

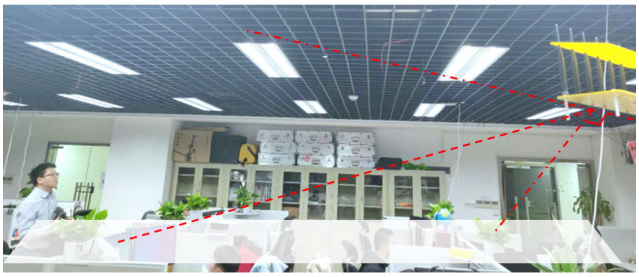

FIGURE 14. Indoor test.

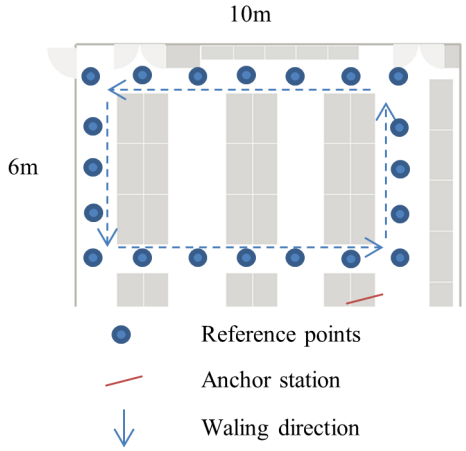

FIGURE 15. Floor plan.

For the problems when the angle approached ±90° for both 6 and 3 antennas, we think it is related to the accuracy of the phase measurement. According to equation (8), the relationship of arccosine leads to a rapid change near the upper and lower bounds. The phase difference approaches to the bounds when the transmitter moves towards the edge, and a slight error leads to a lager variant.

All the results show that AoA estimation based on BLE antennas can achieve high accuracy in a relatively ideal environment with a low multipath effect. The method can be transferred to the indoor environment, which is more valuable than applying in outdoor open space.

B. INDOOR EXPERIMENTS

For the short effective range of BLE, one appropriate application of the single-anchor solution is for positioning in a room-level indoor environment. We implemented the indoor experiment in a typical office, as shown in Fig. 14. The floor plan is shown in Fig. 15.

The tester held the smartphone connected with a PR client. The client was a UWB module with an update rate of 10 Hz. It can transfer ranging data to the phone via the USB in real-time. The tied BLE beacon is independent of the phone. Data with AoA-related information from the receiver array are transmitted back to the phone via its own BLE antenna. An Android app was developed for the test.

The antenna array was placed at a corner of the room to make the most of the effective range, and the height was 2 meters from the ground. The relative height was approxi-

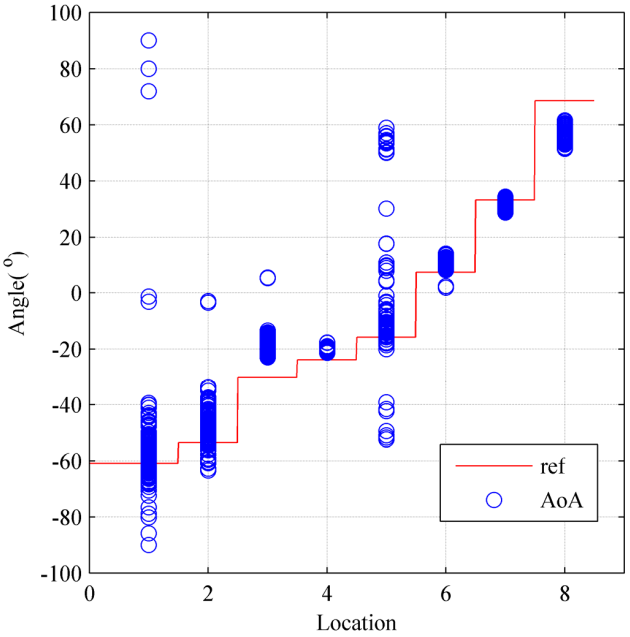

FIGURE 16. AoA estimations indoors for static test.

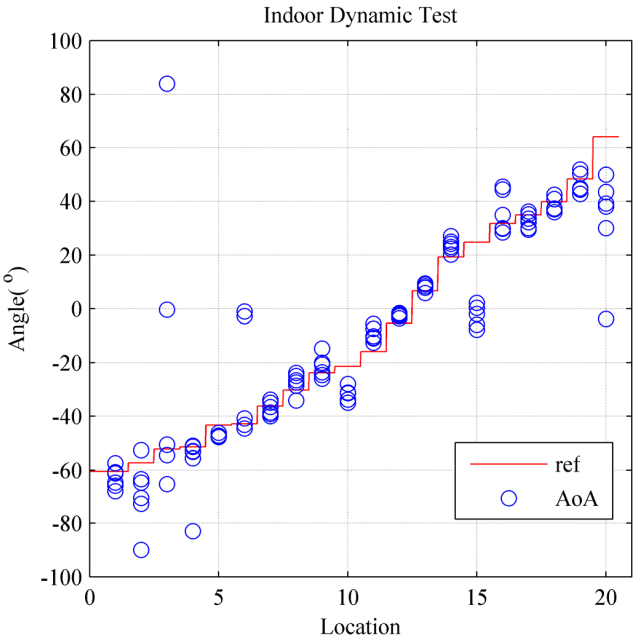

FIGURE 17. AoA estimations indoors for dynamic test.

mately 0.7 meters since the phone was held nearly 1.3 meters high from the ground.

The AoA plane was treated as the same with the floor plane because we considered that the relative height was not too high to distort the angle estimation accuracy.

Twenty reference points around the desks were selected for evaluation. All reference points were measured with a total station.

For individual AoA evaluation indoors, 8 reference locations were selected for the static test. The locations contained 4 corners and 4 aisle midpoints. The tester held the phone and beacon antenna facing the BLE antenna array with no obstructions at these locations, each for 30 seconds. A total of 100 estimations were obtained for each location. The results with 6 antennas are presented in Fig. 16. Reference values are in ascending sort order.

From the results, it is clear that angle measurements could be limited within $\pm 70°$ with the placement of anchor stations. The behavior of the configuration of 6 antennas indoors was not as stable as outdoors. Some locations such as the 3rd position suffered multipath, so that all 100 estimations deviated from the truth.

Multipaths at some locations were reflected in the MUSIC pseudo spectrum, as shown in Fig.8 so that the correct value could be selected by some methods. However, for the static test, the only evidence was the height of the peak, which may lead to a non-direct path. Despite the multipath and other errors, the AoA estimation results were still relatively precise measurements. As Fig. 18 shows, the overall results had an error of approximately $4°$ in 50%, which was not as good as outdoors but is still useful for positioning indoors.

The dynamic test was a rectangular motion of the pedestrian through all 20 reference locations, as shown in Fig. 15.

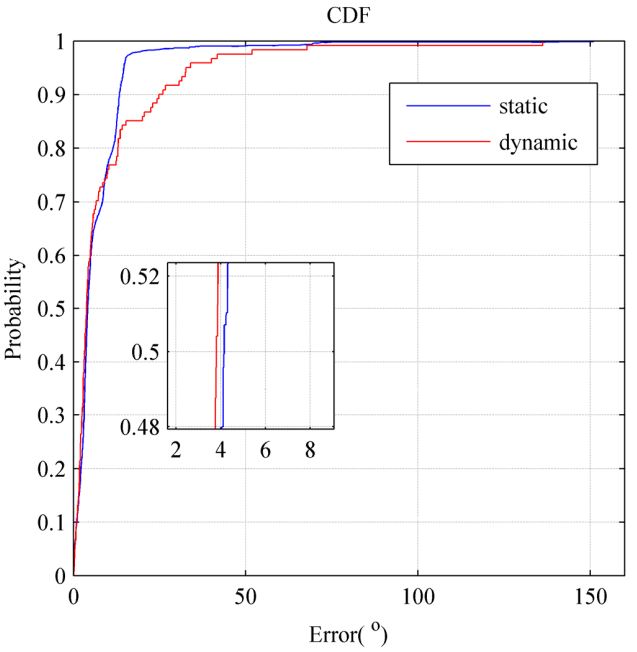

FIGURE 18. CDF of AoA estimations indoors.

The tester held the phone and beacon antenna to walk around the desks. In total, 120 points were evaluated within 6 rounds. A button in the customized app was pushed when arriving at the reference locations to record timestamps, which refer to the standard from NIST [47]. With the timestamps, all related measurements at these locations were extracted for evaluation.

AoA estimations are presented in Fig. 17, and Fig. 18. The results were derived in a dynamic situation, so obstructions such as the body of the tester might appear in some cases; 6 per location and a total of 120 estimations were obtained.

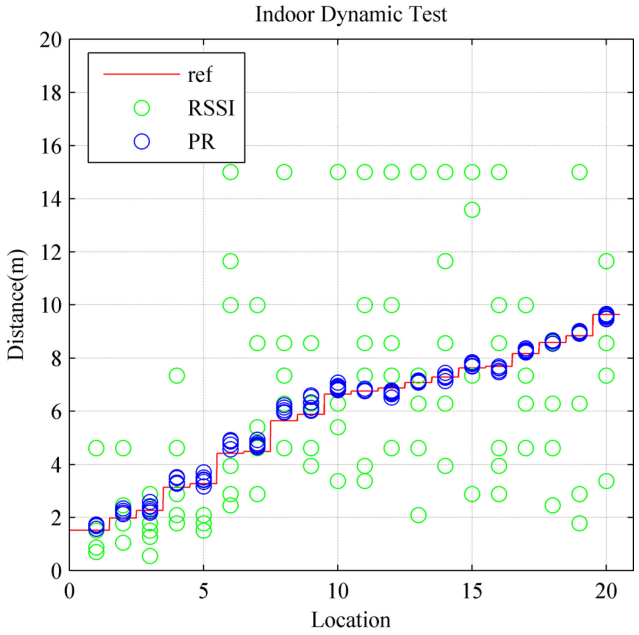

FIGURE 19. Distance measurements.

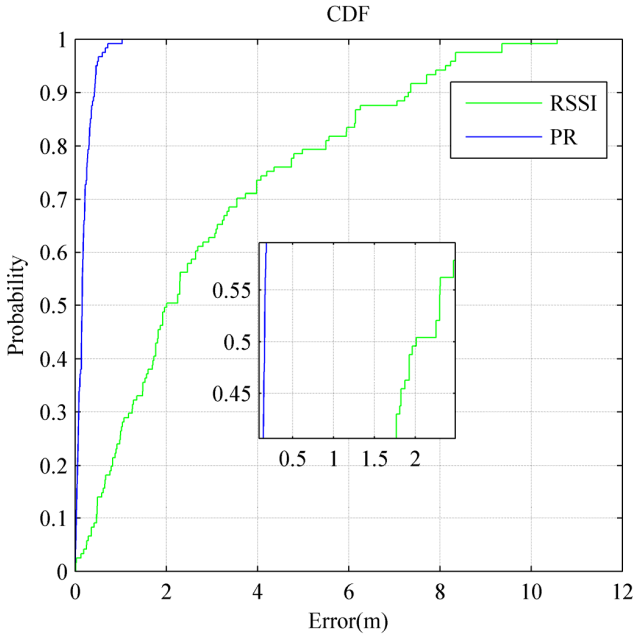

FIGURE 20. CDF of distance measurements.

Angle results with 6 antennas were precise in most locations. However, with the multipath effect and noise, ''flying point'' occurred. There was almost no difference in the mean accuracy between static and dynamic measurements, both with an error of approximately 4°. The total accuracy decreased by approximately 15° in 90% for the static situation and 25° for the dynamic situation. The performance was limited but could be combined with ranging results.

Ranging measurements were only evaluated dynamically, and the results from the PR client and RSSI measurements are shown in Fig.19 and Fig.20.

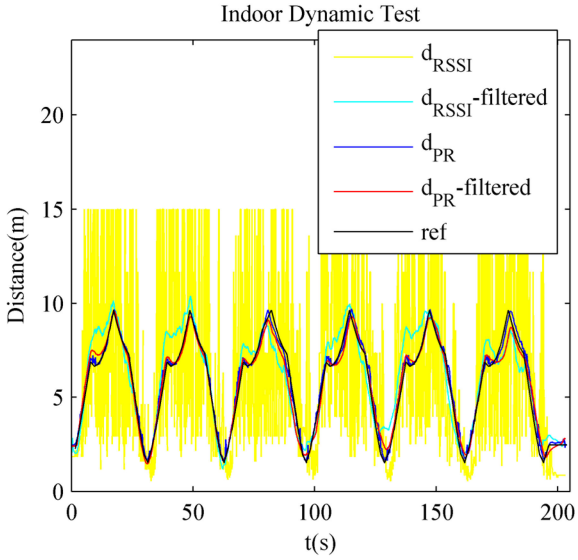

FIGURE 21. Filter effects for distance.

From the figures, it is clear that the high performance of the PR was maintained throughout the entire test. The largest error was approximately 0.5 meters, and the mean error was less than 0.2 meters. The results from RSSI appeal to common sense, which shows less error at close range and large uncertainty at a distant range.

With pairs of AoA and PR or RSSI measurements, positions could be obtained directly. However, errors appeared in too many locations to maintain the trajectory, which decreased the experience.

C. POSITIONING EVALUATION

A PDR constraint was suitable to make the trajectory continuous and smooth. The fusion filter we designed leveraged PDR results as observations. PR or RSSI was applied for distance observation. The PR and RSSI measurements were equivalent to some degree, so it was not necessary to change the structure of the fusion filter when PR and RSSI sources changed.

All data, including BLE, PDR, and PR, were recorded from the same walking trajectory. Two similar filters were implemented simultaneously. We evaluated fusion results from different combinations of sources, including AoA+PR+PDR and AoA+RSSI+PDR.

Fig. 21 shows the raw distance measurements and filtered results from PR and RSSI. Since 6 rounds were walked, a similar form in the records was repeated 6 times.

The errors from PR were originally small, so the effect of filter was not obvious. Burrs of data existed but were controlled by the filter.

For RSSI, the ranging results were strongly filtered. The measurements were so poor that only near and far could be roughly distinguished. Benefiting from fusion with other sources, the filtered results appeared to meet the trajectory. However, a deviation compared to PR still existed.

With the multipath elimination method when fused with PDR, AoA measurements were filtered, as shown in Fig. 22.

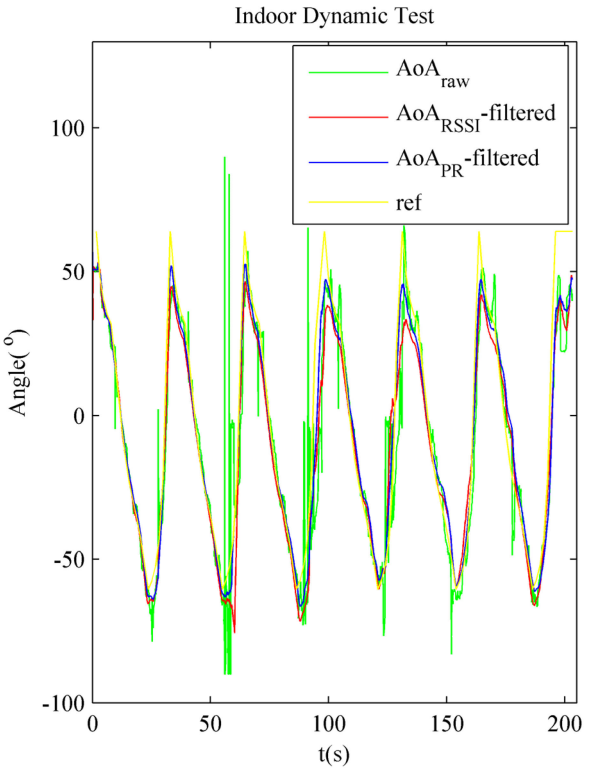

FIGURE 22. Filter effects for AoA.

With the results, we observe that both PR and RSSI measurements combined with PDR can be used to filter the AoA estimations. Additionally, no high latency is introduced. There are some differences between the filtered results from PR and RSSI because the quality of the observations is different. It is clear that the high precision of PR promotes overall performance.

For PDR-related parameters, heading is initialized by the magnetometer with a bias error of nearly 90°. Fusion with absolute sources corrects these biases and gives stable estimations, as shown in Fig.23.

In addition to initial bias, accumulated errors were corrected. It can be seen that the heading calculation result based on gyro accumulates errors over time.

Although the filtered estimations based on RSSI were still not as accurate as those based on PR, both estimations were near the ground truth.

Fig. 24 shows the positions based on PDR, AoA+PR, AoA+PR+PDR, and AoA+RSSI+PDR.

The individual PDR results were almost useless because of their overall deviation from the true trajectory. The results from the AoA+PR combination behaved chaotically because no continuous output from PDR was used. With the PDR constraint, the results of the AoA+PR+PDR and AoA+RSSI+PDR combinations were smooth and continuous.

Fig. 25 shows the CDFs of the positioning error, which is the Euclidean distance between the estimated position and the reference location.

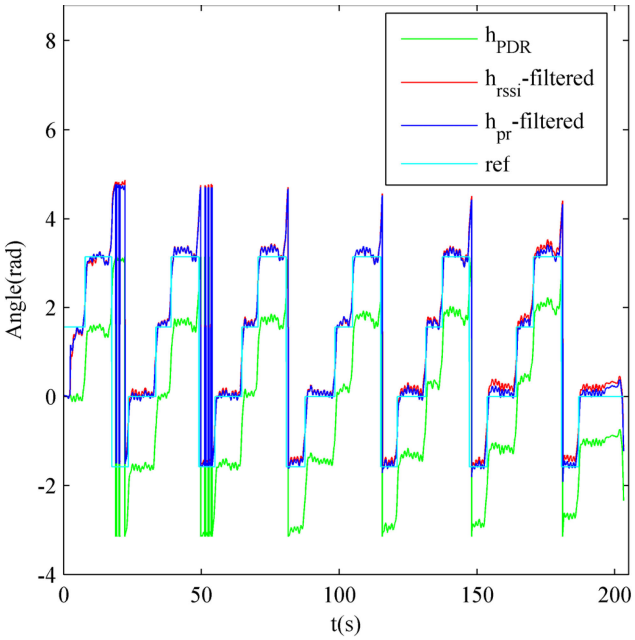

FIGURE 23. Filter effects for heading.

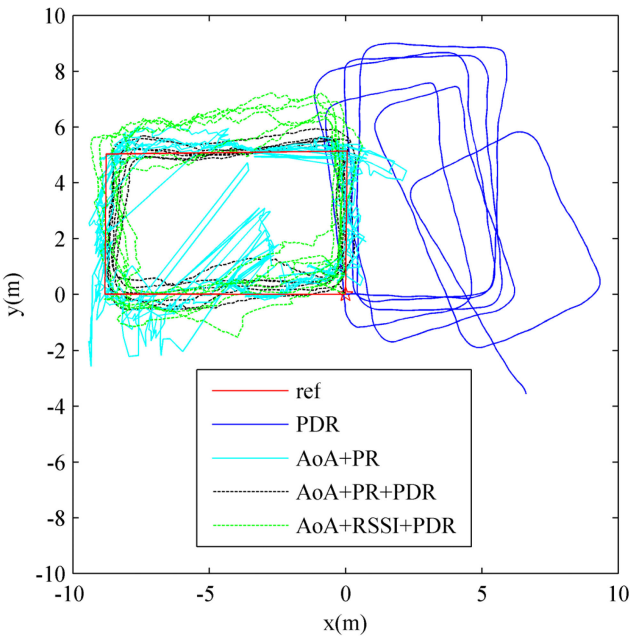

FIGURE 24. Position estimations.

D. IMPROVEMENT WITH MORE ANCHORS

The single anchor can provide positioning services in a room-level area. And the structure is flexible to insert other more anchor stations. That would increase measurements for the system.

The angle estimates and signal strengths from different anchors as Fig. 26 showed can be easily fed into the filter. It can be seen that the whole estimations become smoother with three anchors observed. Fig. 27 shows the comparison of the CDFs with more anchors.

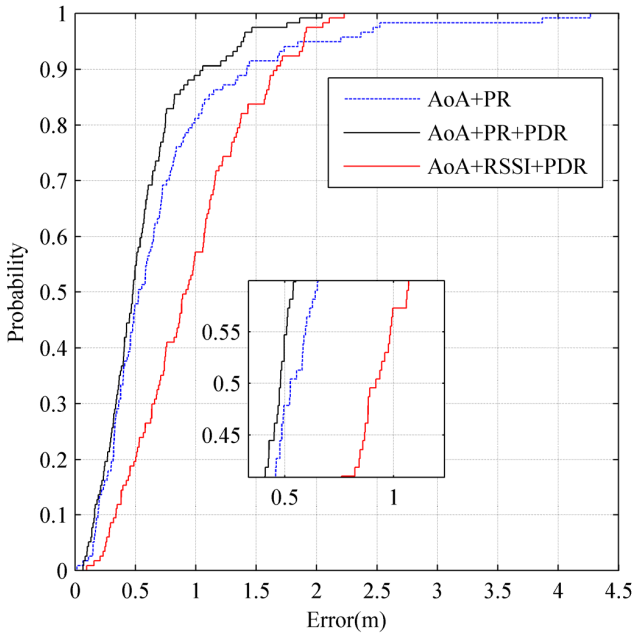

FIGURE 25. CDF of position estimations.

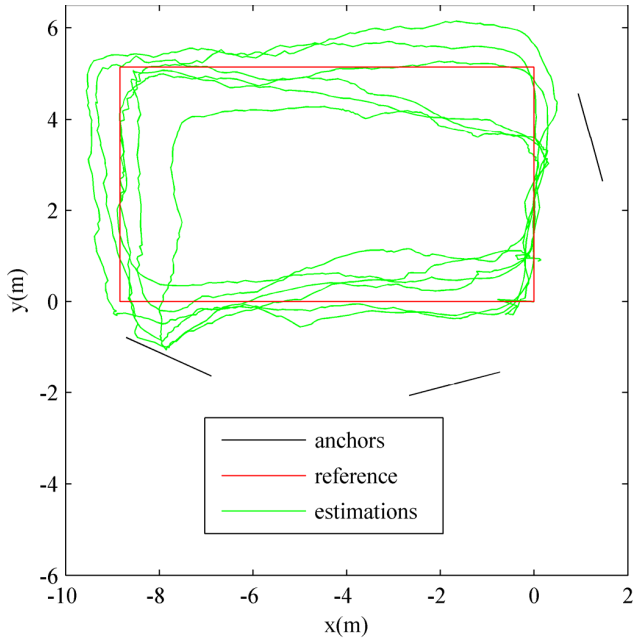

FIGURE 26. Results of three anchors.

The observations from other one or two anchors increase redundancy so that the system can be more robust, but the total accuracy is not promoted too much since the sensors maintain their own system errors. Table 1 shows the specific value of the errors.

From Table 1 and Fig. 25, the best was based on AoA+PR+PDR. Although the mean error of AoA+RSSI+PDR was the highest, large errors did not occur as frequently as with AoA+PR.

The results show that without any PR modules, using AoA and RSSI based on the BLE array could give a mean accuracy

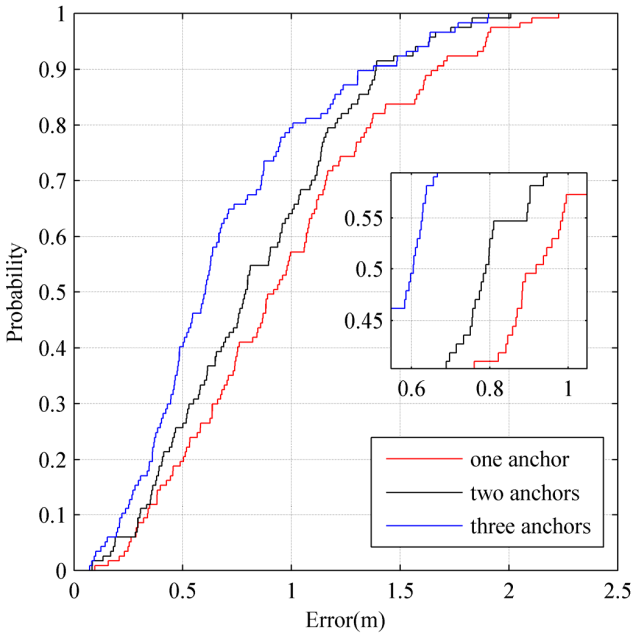

FIGURE 27. CDF of position estimations with multi-anchors.

TABLE 1. Comparison of errors from different combinations.

	Mean(m)	95%(m)	Max(m)
AoA+PR	0.52	2.19	4.27
AoA+PR+PDR	0.48	1.38	2.04
AoA+RSSI+PDR	0.91	1.89	2.23
2*(AoA+RSSI)+PDR	0.79	1.64	2.01
3*(AoA+RSSI)+PDR	0.60	1.63	1.91

of better than 1 meter, which achieved the performance of multi-anchor system.

From Table 1 and Fig. 27, two or more stations improve the performance in the area where they can both cover. And they increase the coverage since an area can provide services in need of signals from only one single-anchor station.

V. CONCLUSION

We proposed a single-anchor solution for indoor positioning. A prototype was implemented. The system takes advantage of the BLE signal to measure the angle and distance. The flexible interfaces of smartphones or other IoT devices make it simple to access additional modules for enhancing the performance. Experiments show that the single-anchor solution works well with a mean error of less than 1 meter in a typical office room, and the performance can be further improved with precise ranging measurements to replace RSSI observations.

Evaluations outdoors indicated that the high-resolution AoA algorithm is precise with 6 antennas and efficient with 3 antennas. The indoor implementation requires 6 antennas for better stability. With these AoA and distance estimations, the PDR results do not need high accuracy. Therefore, it will not increase the computational load or require rigorous high performance of sensors.

Since the BLE transceiver and IMU sensors are common, and the resolution of AoA can be reduced to a more practical level, all the process can be migrated to an embedded platform. A station of rational dimension and a platform for display and computation are the all components for the whole system.

The number of antennas on the station could be decreased for a smaller size to make it more practical. Since 3 antennas have acceptable performance outdoors, the potential of 3 or 4 antenna configurations requires further study. The PR units are expected to be replaced with more universe modules, such as RTT in the newly developed smartphones or ToF from BLE. The only connection between the ranging and angle measuring units is the spatial position, so the station can be customized with minimum changes when carrying different modules.

For a practical smartphone application, the independent BLE transmitter and its rod antenna need to be replaced with the built-in antenna of the phone. The performance of AoA estimation is expected to decrease since the packet rate is lower. For an IoT device, it is not an issue. In future work, we intend to improve the AoA accuracy of the array in a more complex environment and reduce the effect of multipath with fewer antennas.

REFERENCES

[1] N. Zhu, J. Marais, D. Bétaille, and M. Berbineau, "GNSS position integrity in urban environments: A review of literature," *IEEE Trans. Intell. Transp. Syst.*, vol. 99, no. 9, pp. 2762–2778, Sep. 2018.

[2] B. Denby, Y. Oussar, I. Ahriz, and G. Dreyfus, "High-performance indoor localization with full-band GSM fingerprints," in *Proc. ICC*, Dresden, Germany, Jun. 2009, pp. 1–5.

[3] V. Otsason, A. Varshavsky, A. LaMarca, and E. de Lara, "Accurate GSM indoor localization," in *Proc. ICUC*, Berlin, Germany, 2005, pp. 141–158.

[4] B. Li, T. Gallagher, A. G. Dempster, and C. Rizos, "How feasible is the use of magnetic field alone for indoor positioning?" in *Proc. IPIN*, Sydney, NSW, Australia, Nov. 2012, pp. 1–9.

[5] B. Li, T. Gallagher, C. Rizos, and A. G. Dempster, "Using geomagnetic field for indoor positioning," *J. Appl. Geodesy*, vol. 7, no. 4, pp. 299–308, 2013.

[6] C. Yang and H.-R. Shao, "WiFi-based indoor positioning," *IEEE Commun. Mag.*, vol. 53, no. 3, pp. 150–157, Mar. 2015.

[7] Y. Zhuang, Y. Li, L. Qi, H. Lan, N. El-Sheimy, and J. Yang, "A two-filter integration of MEMS sensors and WiFi fingerprinting for indoor positioning," *IEEE Sensors J.*, vol. 16, no. 13, pp. 5125–5126, Jul. 2016.

[8] A. Bose and C. H. Foh, "A practical path loss model for indoor WiFi positioning enhancement," in *Proc. ICICS*, Singapore, Dec. 2007, pp. 1–5.

[9] C. Yang, T. Nguyen, and E. Blasch, "Mobile positioning via fusion of mixed signals of opportunity," *IEEE Aerosp. Electron. Syst. Mag.*, vol. 29, no. 4, pp. 34–46, Apr. 2014.

[10] T. A. Webb, P. D. Groves, P. A. Cross, R. J. Mason, and J. H. Harrison, "A new differential positioning method using modulation correlation of signals of opportunity," in *Proc. IEEE/ION PLANS*, Indian Wells, CA, USA, May 2010, pp. 972–981.

[11] V. Moghtadaiee, S. Lim, and A. G. Dempster, "System-level considerations for signal-of-opportunity positioning," in *Proc. Int. Symp. GPS/GNSS*, Taipei, Taiwan, 2010, pp. 1–7.

[12] K. Batstone, M. Oskarsson, and K. Åström, "Robust time-of-arrival self calibration and indoor localization using Wi-Fi round-trip time measurements," in *Proc. ICC*, Kuala Lumpur, Malaysia, May 2016, pp. 26–31.

[13] M. Ibrahim, H. Liu, M. Jawahar, V. Nguyen, M. Gruteser, R. Howard, and F. Bai, "Verification: Accuracy evaluation of WiFi fine time measurements on an open platform," in *Proc. MobiCom*, New Delhi, India, 2018, pp. 417–427.

[14] G. Giorgetti, A. Cidronali, S. K. S. Gupta, and G. Manes, "Single-anchor indoor localization using a switched-beam antenna," *IEEE Commun. Lett.*, vol. 13, no. 1, pp. 58–60, Jan. 2009.

[15] M. Rzymowski, P. Woznica, and L. Kulas, "Single-anchor indoor localization using ESPAR antenna," *IEEE Antennas Wireless Propag. Lett.*, vol. 15, pp. 1183–1186, Nov. 2015.

[16] M. Kotaru, K. Joshi, D. Bharadia, and S. Katti, "Spotfi: Decimeter level localization using WiFi," in *Proc. SIGCOMM*, New York, NY, USA, 2015, pp. 269–282.

[17] Y. Chen, S. Lu, H.-S. Kim, D. Blaauw, R. G. Dreslinski, and T. Mudge, "A low power software-defined-radio baseband processor for the Internet of Things," in *Proc. IEEE Int. Symp. HPCA*, Mar. 2016, pp. 40–51.

[18] A. Poulose, O. S. Eyobu, and D. S. Han, "An indoor position-estimation algorithm using smartphone IMU sensor data," *IEEE Access*, vol. 7, pp. 11165–11177, 2019.

[19] P. Vorst, J. Sommer, C. Hoene, P. Schneider, C. Weiss, T. Schairer, W. Rosenstiel, A. Zell, and G. Carle, "Indoor positioning via three different RF technologies," in *Proc. 4th Eur. Workshop RFID Syst. Technol.*, Freiburg, Germany, Jun. 2008, pp. 1–10.

[20] S. Xia, Y. Liu, G. Yuan, M. Zhu, and Z. Wang, "Indoor fingerprint positioning based on Wi-Fi: An overview," *ISPRS Int. J. Geo-Inf.*, vol. 6, no. 5, p. 135, Apr. 2017.

[21] P. Bahl and V. N. Padmanabhan, "RADAR: An in-building RF-based user location and tracking system," in *Proc. INFOCOM*, Tel Aviv, Israel, Mar. 2000, pp. 775–784.

[22] M. Youssef and A. Agrawala, "The Horus WLAN location determination system," in *Proc. MobiSys*, Seattle, WA, USA, 2005, pp. 205–218.

[23] K. Al Nuaimi and H. Kamel, "A survey of indoor positioning systems and algorithms," in *Proc. IIT*, Abu Dhabi, United Arab Emirates, Apr. 2011, pp. 185–190.

[24] A. Thaljaoui, T. Val, N. Nasri, and D. Brulin, "BLE localization using RSSI measurements and iRingLA," in *Proc. ICIT*, Seville, Spain, Mar. 2015, pp. 2178–2183.

[25] J. Yang, Z. Wang, and X. Zhang, "An ibeacon-based indoor positioning systems for hospitals," *Int. J. Smart Home*, vol. 9, no. 7, pp. 161–168, 2015.

[26] X.-Y. Lin, T.-W. Ho, C.-C. Fang, Z.-S. Yen, B.-J. Yang, and F. Lai, "A mobile indoor positioning system based on iBeacon technology," in *Proc. EMBS*, Milano, Italy, Aug. 2015, pp. 4970–4973.

[27] A. T. Mariakakis, S. Sen, J. Lee, and K.-H. Kim, "SAIL: Single access point-based indoor localization," in *Proc. MobiSys*, Bretton Woods, NH, USA, 2014, pp. 315–328.

[28] Z.-G. Wu, Z.-L. Deng, and W. Liu, "Simulation of fusion localization based on a single WiFi AP and PDR," in *Proc. MMSTA*, Xiamen, China, 2017, pp. 188–195.

[29] Y. Li, Y. Zhuang, H. Lan, P. Zhang, X. Niu, and N. El-Sheimy, "Self-contained indoor pedestrian navigation using smartphone sensors and magnetic features," *IEEE Sensors J.*, vol. 16, no. 19, pp. 7173–7182, Oct. 2016.

[30] J. Collin, O. Mezentsev, and G. Lachapelle, "Indoor positioning system using accelerometry and high accuracy heading sensors," in *Proc. ION GPS/GNSS*, Portland, OR, USA, 2003, pp. 9–12.

[31] A. R. Jiménez, F. Seco, J. C. Prieto, and J. Guevara, "Indoor pedestrian navigation using an INS/EKF framework for yaw drift reduction and a foot-mounted IMU," in *Proc. WPNC*, Dresden, Germany, Mar. 2010, pp. 135–143.

[32] D. Dardari, P. Closas, and D. M. Djuric, "Indoor tracking: Theory, methods, and technologies," *IEEE Trans. Veh. Technol.*, vol. 64, no. 4, pp. 1263–1278, Apr. 2015.

[33] S. Aparicio, J. Pérez, A. M. Bernardos, and J. R. Casar, "A fusion method based on Bluetooth and wlan technologies for indoor location," in *Proc. MFI*, Seoul, South Korea, Aug. 2008, pp. 487–491.

[34] R. Ma, Q. Guo, C. Hu, and J. Xue, "An improved WiFi indoor positioning algorithm by weighted fusion," *Sensors*, vol. 15, no. 9, pp. 21824–21843, 2015.

[35] A. Colombo, D. Fontanelli, D. Macii, and L. Palopoli, "Flexible indoor localization and tracking based on a wearable platform and sensor data fusion," *IEEE Trans. Instrum. Meas.*, vol. 63, no. 4, pp. 864–876, Apr. 2014.

[36] T. Gaedeke, M. Johnson, M. Hedley, and W. Stork, "Fusion of wireless ranging and inertial sensors for precise and scalable indoor localization," in *Proc. ICC*, Sydney, NSW, Australia, Jun. 2014, pp. 138–143.

[37] L. Chen, L. Pei, H. Kuusniemi, Y. Chen, T. Kröger, and R. Chen, "Bayesian fusion for indoor positioning using Bluetooth fingerprints," *Wireless Pers. Commun.*, vol. 70, no. 4, pp. 1735–1745, 2013.

[38] H. Wang, H. Lenz, A. Szabo, J. Bamberger, and U. D. Hanebeck, "WLAN-based pedestrian tracking using particle filters and low-cost MEMS sensors," in *Proc. WPNC*, Hannover, Germany, Mar. 2007, pp. 1–7.
[39] M. Schüssel, "Angle of arrival estimation using WiFi and smartphones," in *Proc. IPIN*, Sapporo, Japan, 2016, p. 7.
[40] S. M. Alavi, "All-digital I/Q RF-DAC," Ph.D. dissertation, Dept. Elect. Eng., Delft Univ. Technol., Delft, The Netherlands, 2014.
[41] A. Vesa, "Direction-of-arrival estimation in case of uniform sensor array using the MUSIC algorithm," *Trans. Electron. Commun.*, vol. 56, no. 70, pp. 40–43, 2011.
[42] S. N. Bhuiya, F. Islam, and M. A. Matin, "Analysis of direction of arrival techniques using uniform linear array," *Int. J. Comput. Theory Eng.*, vol. 4, no. 6, pp. 931–934, 2012.
[43] L. Brás, N. B. Carvalho, P. Pinho, L. Kulas, and K. Nyka, "A review of antennas for indoor positioning systems," *Int. J. Antennas Propag.*, vol. 2012, Oct. 2012, Art. no. 953269.
[44] R. O. Schmidt, "Multiple emitter location and signal parameter estimation," *IEEE Trans. Antennas Propag.*, vol. 34, no. 3, pp. 276–280, Mar. 1986.
[45] J. Xiong and K. Jamieson, "ArrayTrack: A fine-grained indoor location system," in *Proc. 10th USENIX Symp. Netw. Syst. Design Implement. (NSDI)*, 2013, pp. 71–84.
[46] S. H. Shin, C. G. Park, J. W. Kim, H. S. Hong, and J. M. Lee, "Adaptive step length estimation algorithm using low-cost MEMS inertial sensors," in *Proc. SAS*, San Diego, CA, USA, Feb. 2007, pp. 1–5.
[47] N. Moayeri, M. O. Ergin, F. Lemic, V. Handziski, and A. Wolisz, "PerfLoc: A comprehensive repository of experimental data for evaluation of smartphone indoor localization apps," presented at the 2nd KuVS Expert Talk Localization, Lübeck, Germany, Jul. 2016.

FENG YE received the B.S. degree in automation and the M.S. degree in optical engineering from Huazhong University of Science and Technology, China, in 2014 and 2017, respectively. He is currently pursuing the Ph.D. degree in the geodesy and survey engineering, Wuhan University, Wuhan, China. His research interests include indoor positioning, ubiquitous computing, machine learning, and the Internet of Things.

RUIZHI CHEN is currently a Professor and the Director of the State Key Laboratory of Information Engineering in Surveying, Mapping and Remote Sensing with Wuhan University. He was an Endowed Chair Professor with Texas A&M University Corpus Christi, Corpus Christi, TX, USA, the Head and a Professor of the Department of Navigation and Positioning with the Finnish Geodetic Institute, Finland, and an Engineering Manager with Nokia, Finland. He has published two books and more than 200 scientific articles. His current research interests include indoor positioning, satellite navigation, and location-based services.

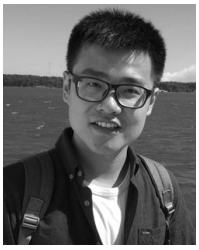

GUANGYI GUO received the B.S. degree in geographic information science and the M.S. degree in geographic information science from Hubei University, China, in 2012 and 2015, respectively. He is currently pursuing the Ph.D. degree in the cartology and geographical information science, Wuhan University, Wuhan, China. His research interests include indoor positioning, machine learning, and the Internet of Things.

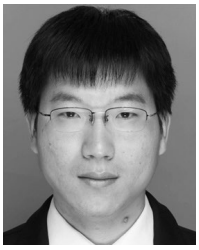

XUESHENG PENG received the B.S. degree in Lan Resources Management from Wuhan University, China, in 2014, and the M.S. degree in surveying and mapping engineering from Henan Polytechnic University, China, in 2017. He is currently pursuing the Ph.D. degree in the geodesy and survey engineering, Wuhan University. His research interests include indoor positioning and the Internet of Things.

ZUOYA LIU received the B.S. degree in electronic information science and technology and the M.S. degree in electronic circuit and system from Central China Normal University, China, in 2012 and 2015, respectively. He is currently pursuing the Ph.D. degree in the cartology and geographical information science, Wuhan University, Wuhan, China. His research interests include indoor positioning, navigation, machine learning, and the Internet of Things.

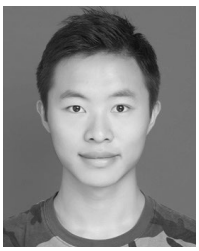

LIXIONG HUANG received the B.S. degree in geodesy and geomatics engineering from Wuhan University, China, in 2019, and he is about to further his study at Wuhan University. His research interests include indoor positioning, the Internet of Things, and information fusion.